Statistical mechanics of strongly correlated Bose quantum fluids

B. E. Clements, E. Krotscheck, and J. A. Smith
Center for Theoretical Physics and Department of Physics, Texas A&M University, College Station, Texas 77843

C. E. Campbell
School of Physics and Astronomy, University of Minnesota, Minneapolis, Minnesota 55455
(Received 10 June 1992)

The finite-temperature properties of Bose quantum fluids are studied by applying a variational density-matrix approach. Our ansatz for the density matrix is similar to that introduced by Campbell, Kürten, Ristig, and Senger [Phys. Rev. **30**, 3728 (1984)] but has been generalized to include three-body correlations. An expression for the finite-temperature elementary-excitation energy, $\epsilon(k)$, is derived from an ansatz for the variational entropy. At zero temperature $\epsilon(k)$ reduces to the same expression obtained by Brillouin-Wigner perturbation theory. The hypernetted-chain (HNC) equations provide the relations between the n-particle distribution functions and the correlation functions. A substantial set of elementary diagrams have been included to minimize the loss of precision associated with the HNC approximation. We report values for the static structure function, radial distribution function, excitation energies, particle-hole interaction, Helmholtz free energy, entropy, and isothermal sound velocity. We present a detailed study of the spectra, three-body correlations, and elementary diagram dependence of the thermodynamic spinodal curve. For relevant densities, we find that three-body correlations tend to increase the liquid-gas critical temperature T_c while adding elementary diagrams tends to reduce T_c. Including multiphonon terms in the spectrum produces several features in the variational entropy that were not observed at the Feynman level of excitations. Entropy isotherms show a rather abrupt transition from a low-density regime, where multiphonon contributions are insignificant, to a high-density regime where the isotherms are strongly influenced by multiphonon scattering processes.

I. INTRODUCTION

Recently, high-precision neutron-scattering measurements have been done in superfluid and normal ^{4}He at saturated vapor pressure (SVP) by Stirling and Glyde,[1] and at 20 bars by Talbot *et al.*[2] Momentum transfers of $Q = 0.4$ and 1.925 Å^{-1} were probed. In the Feynman theory of elementary excitations in ^{4}He, these wave vectors correspond to that of a phonon and the roton minimum, respectively. As a result of these measurements precise data are now available for the temperature dependence of the dynamic structure function $S(Q,\omega)$. Stirling and Glyde report the following: For $Q=$ 0.4 Å^{-1}, $S(Q,\omega)$ contains a single sharp peak, the well-known Bijl-Feynman (BF) phonon-roton collective mode. This peak is superimposed on a nearly temperature-independent broad background, which originates from the quasiparticle-quasiparticle scattering (multiphonon contributions). The Bijl-Feynman peak broadens and diminishes in strength as the temperature is increased through the λ transition temperature T_λ (T_λ=2.17 K at SVP) but does not fully vanish into the background until the system is deep into the normal phase. At the roton minimum, the sharp component in $S(Q,\omega)$ has a noticeably different temperature dependence; it vanishes or at least changes abruptly as the temperature is increased through T_λ. This confirmed earlier observations of Woods and Svensson.[3]

These experimental observations led Glyde and Griffin[4] to propose a novel interpretation of the excitations in liquid ^{4}He. Using the dielectric formulation of many-body theory,[5] they suggest that phonons ($Q \leq 0.7$ Å^{-1}) and rotons ($Q \approx 1.9$ Å^{-1}) really involve separate excitation branches, which are hybridized by the presence of the Bose condensate. As a result of the level crossing, the lowest-lying excitations are those observed in the experimental phonon-maxon-roton spectrum, but the nature of the excitation depends critically on the wave vector.

This picture differs from the traditionally accepted picture of the experimental BF spectrum being a density fluctuation (collective mode) not only in the phonon regime, but for wave vectors extending beyond the roton minimum. This interpretation, which originated with Feynman, has been supported by numerous theoretical calculations.[6–12] In this picture, while the condensate is present, it is assumed to have no special connection with the low-lying elementary excitations. The present work is based on this interpretation of the spectrum.

It remains a challenge for the low-temperature physicist to reconcile the traditional picture with the convincing arguments proposed by Glyde and Griffin. The dielectric formulation has the advantage that it works equally well for zero- and finite-temperature many-body systems. In contrast, all correlated basis functions (CBF) and variational calculations done to the degree of preci-

sion needed to resolve these issues have been done at zero temperature only. One of the goals of this work is to extend to higher precision, previous finite-temperature calculations based on a variational principle. While the presently investigated density matrix provides a proper description of the superfluid only, and thus precludes the possibility of studying the superfluid-normal transition needed to reconcile the two pictures, it is a necessary step in the development of statistical mechanics for strongly correlated systems.

The solution to the many-body problem by a variational approach was extended to finite temperatures in the pioneering work of Campbell *et al.*[13] At the heart of that work is the Gibbs-Delbrück-Moliere minimum principle for the Helmholtz free energy. The principle states that the trial Helmholtz free energy F_t is bounded from below by the true free energy F_0 and is given by

$$F_0 \leq F_t = \mathrm{tr}(H\rho_t) + \frac{1}{\beta}\mathrm{tr}(\rho_t \ln \rho_t), \tag{1.1}$$

where $\beta = 1/k_B T$, H is the many-body Hamiltonian, and ρ_t is a trial density matrix. The first and second terms are contributions to the free energy coming from the trial internal energy and entropy, respectively. In configuration space H is given by

$$H = -\frac{\hbar^2}{2m}\sum_{i=1}^{N}\nabla_i^2 + \sum_{i<j} v(|\,\mathbf{r}_i - \mathbf{r}_j\,|), \tag{1.2}$$

where m is the bare mass of the Bose particle and $v(r)$ is a two-body interaction potential. [In our numerical calculations, $v(r)$ is the potential of Aziz *et al.*[14]]

The density matrix introduced by Campbell *et al.*, and discussed in more detail below, is called the Penrose-Reatto-Chester-Jastrow (PRCJ) density matrix.[15] It is expressible entirely in terms of two-body variational functions:

$$\rho_t \sim \exp\left[\frac{1}{2}\sum_{i<j} u_2(\mathbf{r}_i, \mathbf{r}_j)\right] \exp\left[\frac{1}{2}\sum_{i,j} \omega_2(\mathbf{r}_i, \mathbf{r}'_j)\right] \exp\left[\frac{1}{2}\sum_{i<j} u_2(\mathbf{r}'_i, \mathbf{r}'_j)\right]. \tag{1.3}$$

At zero temperature ω_2 vanishes and ρ_t reduces to a product of Jastrow wave functions. The optimal free energy follows after solving a set of coupled Euler-Lagrange (EL) equations:

$$\left.\frac{\delta F_t}{\delta u_2}\right|_{\omega_2} = 0, \quad \left.\frac{\delta F_t}{\delta \omega_2}\right|_{u_2} = 0, \tag{1.4}$$

a calculation that is similar in spirit to that used to find the optimal ground-state energies in the zero temperature limit.[16] Solutions to these equations were used to study the temperature dependence of the elementary-excitation spectrum. In the following work of Senger *et al.*,[17] the thermal behavior of microscopic quantities such as the static structure function $S(k)$ and the isothermal sound velocity was calculated. They also calculated many thermodynamic functions including the Helmholtz free energy, internal energy, entropy, pressure, and the chemical potential. The solutions of the EL equations fail to give (unphysical) solutions in regions of phase space that are mechanically unstable (regions of diverging compressibility). Consequently, they were able to determine the thermodynamic spinodal curve.

The qualitative success of those calculations provided incentive for further work: The procedure has been extended to include Bose mixtures[18] and inhomogeneous Bose systems.[19] A density matrix, which properly describes the normal phase (temperatures above the λ transition) has been postulated, and EL equations have been derived.[15,17,20] Finally, an alternative formulation, which results in exact expressions for the EL equations for the PRCJ density matrix, has been introduced.[21]

Yet another line to follow, which is the intent of the present work, is to extend the PRCJ density matrix by adding three-body correlations to both the u and the ω. In Sec. II, we introduce the extended PRCJ density matrix. Closed form expressions for the internal energy and entropy are derived in Sec. III. EL equations are derived in Sec. IV. In doing so, we show that a finite-temperature version of the Brillouin-Wigner (BW) perturbation theory excitation spectrum follows from the EL equations. Having the BW expression for $\epsilon(k)$ emerge from the formalism adds credence to the method employed for introducing the spectrum, which is through the entropy expression. The present work goes beyond that previously done in another important way. In the evaluation of the EL equations it is necessary to invoke the hypernetted-chain (HNC) resummation of diagrams. We have included a set of elementary diagrams that are consistent with keeping u_3 correlations. In earlier finite-temperature calculations these have been ignored. Keeping u_3 and elementary diagrams is known to be important in obtaining correct ground-state properties.[22,23] A brief review of the thermodynamic functions studied in this work are given in Sec. V. Numerical solutions are given in Sec. VI, and conclusions are stated in Sec. VII. We begin by reviewing the density matrix formalism.

II. DENSITY MATRIX

At finite temperature a many-body quantum system is completely determined by the statistical density matrix $\hat{\rho}$. As is well known, the expectation value for any operator, θ may be expressed as a quantum-mechanical trace over the product of $\hat{\rho}$ and the operator:

$$\langle\theta\rangle = \mathrm{tr}(\hat{\rho}\theta). \tag{2.1}$$

Since Bose quantum liquids are strongly correlated in configuration space, it is advantageous to expand all state vectors $|\Psi\rangle$ and operators, including $\hat{\rho}$, in terms of real-space basis vectors:

$$\langle \mathbf{r}_1, \ldots, \mathbf{r}_N | \Psi \rangle = \Psi(\mathbf{r}_1, \ldots, \mathbf{r}_N), \tag{2.2}$$

$$\langle \mathbf{r}_1^\alpha, \ldots, \mathbf{r}_N^\alpha | \hat{\rho} | \mathbf{r}_1^\beta, \ldots, \mathbf{r}_N^\beta \rangle = \rho(\mathbf{r}_1^\alpha, \ldots, \mathbf{r}_N^\alpha, \mathbf{r}_1^\beta, \ldots, \mathbf{r}_N^\beta).$$

In the superfluid regime ρ_t may be decomposed into two positive-definite pieces:

$$\rho_t(\mathbf{r}_1^\alpha, \ldots, \mathbf{r}_N^\alpha, \mathbf{r}_1^\beta, \ldots, \mathbf{r}_N^\beta) = \Psi(\mathbf{r}_1^\alpha, \ldots, \mathbf{r}_N^\alpha) Q(\mathbf{r}_1^\alpha, \ldots, \mathbf{r}_N^\alpha, \mathbf{r}_1^\beta, \ldots, \mathbf{r}_N^\beta) \Psi(\mathbf{r}_1^\beta, \ldots, \mathbf{r}_N^\beta), \tag{2.3}$$

where Ψ has the form of the Feenberg wave function:

$$\Psi(\mathbf{r}_1, \ldots, \mathbf{r}_N) = \exp\left(\frac{1}{2} \sum_{i<j} u_2(\mathbf{r}_i, \mathbf{r}_j) + \frac{1}{2} \sum_{i<j<k} u_3(\mathbf{r}_i, \mathbf{r}_j, \mathbf{r}_k) \cdots \right). \tag{2.4}$$

An important distinction exists between Ψ and the true Feenberg wave function in that the latter describes the many-body ground state, while at finite temperature the correlation functions, $u_2, u_3, \ldots$ are temperature dependent. Conversely, the dominating correlations at zero temperature are expected to be equally important at low temperatures. Consequently, one expects that these functions will have a rather weak temperature dependence. At zero temperature Ψ reduces to the ground-state Feenberg wave function. In contrast to Jastrow calculations previously reported,[13,17] in the present work we truncate the u_n series at $n = 3$.

The incoherence function Q couples the $\mathbf{r}^\alpha$ and $\mathbf{r}^\beta$ coordinates. As the temperature approaches zero, Q is expected to go smoothly to unity. The incoherence function currently studied has the form

$$Q(\mathbf{r}_1^\alpha, \ldots, \mathbf{r}_N^\alpha, \mathbf{r}_1^\beta, \ldots, \mathbf{r}_N^\beta) = \exp\left[\frac{1}{2N} \sum_{\mathbf{k}} \omega_2(k) (F_{\mathbf{k}}^\alpha F_{-\mathbf{k}}^\beta + F_{\mathbf{k}}^\beta F_{-\mathbf{k}}^\alpha - F_{\mathbf{k}}^\alpha F_{-\mathbf{k}}^\alpha - F_{\mathbf{k}}^\beta F_{-\mathbf{k}}^\beta) \right], \tag{2.5}$$

where

$$F_{\mathbf{k}}^\alpha = \rho_{\mathbf{k}}^\alpha + \frac{1}{N} \sum_{\mathbf{q}} \frac{\omega_3(\mathbf{q}, \mathbf{k}-\mathbf{q})}{\omega_2(\mathbf{k})} \rho_{\mathbf{q}}^\alpha \rho_{\mathbf{k}-\mathbf{q}}^\alpha. \tag{2.6}$$

The density fluctuation operator, $\rho_{\mathbf{k}}^\alpha$, is the Fourier transform of the local number density operator:

$$\rho_{\mathbf{k}}^\alpha = \sum_{j=1}^{N} e^{i\mathbf{k}\cdot\mathbf{r}_j^\alpha}. \tag{2.7}$$

The density matrix is properly normalized by dividing by the corresponding trial partition function:

$$Z_t = \int d(\mathbf{r}_1, \ldots, \mathbf{r}_N) \Psi^2(\mathbf{r}_1, \ldots, \mathbf{r}_N). \tag{2.8}$$

Equation (2.5) requires a certain amount of discussion in that it is not a straightforward generalization of the form studied by Campbell *et al.* In that work only one variational function, ω_2, was used, tantamount to setting $F_{\mathbf{k}}^\alpha \equiv \rho_{\mathbf{k}}^\alpha$. The most straightforward way to include higher-order correlation functions in the incoherence function would be to include the terms (with the appropriate permutations) $\omega_3(\mathbf{r}_i^\alpha, \mathbf{r}_j^\alpha, \mathbf{r}_k^\beta), \omega_4(\mathbf{r}_i^\alpha, \mathbf{r}_j^\alpha, \mathbf{r}_k^\alpha, \mathbf{r}_l^\beta), \ldots$. The generated series would have the standard "Feenberg form" for the incoherence function. While Eq. (2.5) is a proper representation for the incoherence function, the ratio of ω_3/ω_2 is more closely related to the variational generalization of the "backflow" form used by Battaini and Reatto.[24] The association follows from their Eq. (8):

$$-A_k(4\pi N/V)\mathbf{k}\cdot\mathbf{q}/q^2 \to \omega_3/\omega_2. \tag{2.9}$$

It is immediately apparent from Eq. (2.5) that one obtains higher powers of ω_3/ω_2, revealing that ω_3 cannot itself be regarded as a component of the Feenberg expansion. Equation (2.5) is computationally easier to use, and for that reason it is chosen in the current work.

Finally, the optimal u_n and ω_n for $n = 2, 3$ are determined by the solutions of the EL equations:

$$\frac{\delta F_t}{\delta u_n} = 0, \quad \frac{\delta F_t}{\delta \omega_n} = 0. \tag{2.10}$$

III. INTERNAL ENERGY AND ENTROPY

To perform the functional derivatives required by the optimization conditions [Eq. (2.10)] it is first necessary to find closed-form expressions for the trial internal energy U_t and entropy $\mathcal{S}_t$. The calculation of U_t is facilitated by using the Jackson-Feenberg (JF) expression for the kinetic energy T:

$$T_{\mathrm{JF}} = \frac{\hbar^2}{4m} \sum_{i=1}^{N} (\nabla_i' \cdot \nabla_i - \nabla_i^2) \delta(\mathbf{r}_i - \mathbf{r}_i'), \tag{3.1}$$

where the δ functions are to be evaluated after the action of the gradient. The kinetic-energy contribution may be split into two terms, which can be represented symbolically as

$$[\nabla_1' \cdot \nabla_1 - \nabla_1^2]\Psi(R)Q(R,R')\Psi(R')|_{R=R'}$$
$$= \left[\nabla_1'\Psi(R') \cdot \nabla_1\Psi(R) - \Psi(R')\nabla_1^2\Psi(R)\right]_{R=R'}$$
$$+|\Psi(R)|^2 \left[\nabla_1'\nabla_1 Q(R,R') - \nabla_1^2 Q(R,R')\right]_{R=R'}. \tag{3.2}$$

The internal energy then separates naturally into the following terms:

$$U_t = \mathrm{tr}(H\rho_t) = U_2 + U_{\Delta u} + U_{\omega_2} + U_{\Delta\omega}. \tag{3.3}$$

At zero temperature, Krotscheck[22] has derived expressions for the ground-state energy when the Feenberg wave function [$n = 2$ and 3 in Eq. (2.4)] is used as the variational ansatz. The kinetic energy evaluated by Krotscheck is essentially the first term of Eq. (3.2). We may immediately use the results of that analysis to obtain the correct finite-temperature version,

$$U_2 = \frac{N\rho}{2}\int dr\, g(r)\left[v(r) - \frac{\hbar^2}{4m}\nabla^2[\ln g(r) - N(r)]\right] \tag{3.4}$$

and

$$U_{\Delta u}/N = E_{(3)} + \frac{\hbar^2\rho}{8m}\int dr\, g(r)\nabla^2[E_3(r) + E(r)], \tag{3.5}$$

where

$$E_3(|\mathbf{r}_1 - \mathbf{r}_2|) = \rho\int d\mathbf{r}_3\, g(\mathbf{r}_1,\mathbf{r}_3)g(\mathbf{r}_2,\mathbf{r}_3)u_3(\mathbf{r}_1,\mathbf{r}_2,\mathbf{r}_3) \tag{3.6}$$

and

$$E_{(3)} = -\frac{\hbar^2\rho^3}{48m}\int d\mathbf{r}_1\int d\mathbf{r}_2\int d\mathbf{r}_3[g_3(\mathbf{r}_1,\mathbf{r}_2,\mathbf{r}_3) - g(\mathbf{r}_1,\mathbf{r}_2) - g(\mathbf{r}_1,\mathbf{r}_3) - g(\mathbf{r}_2,\mathbf{r}_3) + 2](\nabla_1^2 + \nabla_2^2 + \nabla_3^2)u_3(\mathbf{r}_1,\mathbf{r}_2,\mathbf{r}_3). \tag{3.7}$$

In these expressions the radial distribution function $g(\mathbf{r}_1,\mathbf{r}_2) = g(|\mathbf{r}_1 - \mathbf{r}_2|)$ is given by

$$g(|\mathbf{r}_1 - \mathbf{r}_2|) = \frac{N(N-1)}{\rho^2}\int d(\mathbf{r}_3,\ldots,\mathbf{r}_N)\rho_t(\mathbf{r}_1,\ldots,\mathbf{r}_N;\mathbf{r}_1,\ldots,\mathbf{r}_N). \tag{3.8}$$

The nodal and elementary functions $N(r)$ and $E(r)$ in Eqs. (3.4) and (3.5) follow from the (exact) hypernetted-chain representation of $g(r)$:

$$g(r) = e^{u_2(r)+N(r)+E_3(r)+E(r)}, \tag{3.9}$$

$$N(r) = \frac{1}{(2\pi)^3\rho}\int d\mathbf{k}\, e^{-i\mathbf{k}\cdot\mathbf{r}}\frac{[S(k)-1]^2}{S(k)}, \tag{3.10}$$

where equations are generalized to include the presence of three-body correlations:[22] These equations are consistent with the well-known relation that exists between $g(r)$ and the static structure function $S(k)$:

$$S(k) = 1 + \rho\int dr\, e^{i\mathbf{k}\cdot\mathbf{r}}[g(r) - 1]. \tag{3.11}$$

The ω dependence follows from the second term of Eq. (3.2). The result is

$$U_\omega = \frac{\hbar^2}{2mZ_t}\sum_{\mathbf{k}}\omega_2(k)\langle\Psi|\nabla_1 F_{\mathbf{k}}\cdot\nabla_1 F_{-\mathbf{k}}|\Psi\rangle. \tag{3.12}$$

Expanding the $F_{\mathbf{k}}$, as in Eq. (2.6), separates the internal energy contributions into a term that depends on ω_2 only,

$$U_{\omega_2} = \sum_{\mathbf{k}}\epsilon_0(k)\omega_2(k), \tag{3.13}$$

where $\epsilon_0(k) = \hbar^2k^2/2m$, and terms involving the three-body dependence of the incoherence function,

$$U_{\Delta\omega} = \frac{1}{Z_tN^2}\sum_{\mathbf{k},\mathbf{q}}[\omega_3(\mathbf{q},\mathbf{k}-\mathbf{q})\langle\Psi|\rho_{\mathbf{q}}\rho_{\mathbf{k}-\mathbf{q}}(H-E_0)\rho_{-\mathbf{k}}|\Psi\rangle + (\mathbf{k}\to-\mathbf{k})]$$
$$+\frac{1}{Z_tN^3}\sum_{\mathbf{k},\mathbf{q},\mathbf{p}}\frac{\omega_3(\mathbf{q},\mathbf{k}-\mathbf{q})\omega_3(-\mathbf{p},\mathbf{p}-\mathbf{k})}{\omega_2(k)}\langle\Psi|\rho_{\mathbf{q}}\rho_{\mathbf{k}-\mathbf{q}}(H-E_0)\rho_{-\mathbf{p}}\rho_{\mathbf{p}-\mathbf{k}}|\Psi\rangle. \tag{3.14}$$

In this equation $E_0 \equiv \langle\Psi|H|\Psi\rangle/Z_t$.

The calculation of the trial entropy $\mathcal{S}_t$ is a straightforward generalization of the entropy calculation in Refs. 13 and 17. Following that work, we know that it is possible to map the entropy expression onto the evaluation of a σ-component configuration integral by using the replica identity

$$\mathcal{S}_t = -k_B \, \mathrm{tr}(\rho_t \ln \rho_t) \equiv -k_B \frac{d}{d\sigma} \ln \mathrm{tr}(\rho_t^\sigma)\Big|_{\sigma=1}. \tag{3.15}$$

The trace of powers of the density matrix can be written in the compact form

$$\mathrm{tr}(\rho_t^\sigma) = \frac{1}{Z_t^\sigma} \int \prod_{\nu=1}^{\sigma} \{d(\mathbf{r}_1^\nu, \ldots, \mathbf{r}_N^\nu)\Psi^2(\mathbf{r}_1^\nu, \ldots, \mathbf{r}_N^\nu)\} \prod_{\mathbf{k}>0} \exp\left(\frac{1}{N} \sum_{\alpha,\beta=1}^{\sigma} F_{\mathbf{k}}^\alpha M_{\alpha\beta} F_{-\mathbf{k}}^\beta\right), \tag{3.16}$$

where $\underline{M}$ is a $\sigma \times \sigma$ matrix,

$$M_{\alpha\beta}(\mathbf{k};\sigma) = \omega_2(k)\{\delta_{\alpha,\beta+1}(\sigma) + \delta_{\alpha+1,\beta}(\sigma) - 2\delta_{\alpha,\beta}(\sigma)\}. \tag{3.17}$$

The Kronecker δ functions obey the cyclic condition that $\delta_{\alpha,\beta+\sigma}(\sigma) = \delta_{\alpha,\beta}(\sigma)$. The many-body integral in Eq. (3.16), with $\rho_{\mathbf{k}}$ in place of $F_{\mathbf{k}}$, was evaluated by invoking a separability approximation.[17] Consequently, we may immediately apply the analysis of Ref. 17 to find a closed-form expression for the entropy. We simply state the results. Relating the variational functions to the momentum distribution $n(k)$,

$$\begin{aligned} n(k)(n(k)+1) &= \frac{1}{Z_t N}\omega_2(k)\langle\Psi|F_{\mathbf{k}}F_{-\mathbf{k}}|\Psi\rangle \\ &= \frac{1}{Z_t N}\omega_2(k)\langle\Psi|\rho_{\mathbf{k}}\rho_{-\mathbf{k}}|\Psi\rangle + \frac{1}{Z_t N^2}\sum_{\mathbf{q}}[\omega_3(\mathbf{q},\mathbf{k}-\mathbf{q})\langle\Psi|\rho_{\mathbf{q}}\rho_{\mathbf{k}-\mathbf{q}}\rho_{-\mathbf{k}}|\Psi\rangle + (\mathbf{k}\to-\mathbf{k})] \\ &\quad + \frac{1}{Z_t N^3}\sum_{\mathbf{q},\mathbf{p}} \frac{\omega_3(\mathbf{q},\mathbf{k}-\mathbf{q})\omega_3(-\mathbf{p},\mathbf{p}-\mathbf{k})}{\omega_2(k)}\langle\Psi|\rho_{\mathbf{q}}\rho_{\mathbf{k}-\mathbf{q}}\rho_{-\mathbf{p}}\rho_{\mathbf{p}-\mathbf{k}}|\Psi\rangle, \end{aligned} \tag{3.18}$$

allows the entropy to be cast in the form of a gas of noninteracting Bose quasiparticles:

$$\mathcal{S}_t = k_B \sum_{\mathbf{k}}\{[n(k)+1]\ln[n(k)+1] - n(k)\ln n(k)\}. \tag{3.19}$$

We may now introduce the elementary-excitation energies $\epsilon(k)$:

$$n(k) = \frac{1}{e^{\beta\epsilon(k)}-1}. \tag{3.20}$$

An important point is that while we assume Eq. (3.19) remains correct when three-body correlations are accounted for, we expect that $\epsilon(k)$ will no longer be the finite-temperature version of the Feynman spectrum, but rather will be modified by higher-order self-energy corrections:

$$\epsilon(k) = \epsilon_{\mathrm{BF}}(k) + \Sigma(k,\epsilon(k)). \tag{3.21}$$

In Sec. IV, where the EL equations are derived, we will show that Σ is a finite-temperature generalization of that obtained from second-order Brillouin-Wigner perturbation theory. A discussion of the thermodynamic conditions for which Eq. (3.19) can be expected to be reliable is deferred to Sec. VI.

IV. EULER-LAGRANGE EQUATIONS

Having obtained closed-form expressions for the Helmholtz free energy, one can immediately evaluate the functional derivatives in Eq. (2.10). It has become standard to choose $g(r)$ rather than u_2 for an independent variational function. We begin with the ω_2 and ω_3 EL equations. Functional differentiation leads to the coupled set of equations,

$$\frac{\delta F_t}{\delta\omega_2(k)}\Big|_{g,u_3,\omega_3} = 0 = \epsilon_0(k) - \epsilon^*(k)S(k) - \frac{1}{Z_t N^3}\sum_{\mathbf{q},\mathbf{p}} \frac{\omega_3(\mathbf{q},\mathbf{k}-\mathbf{q})\omega_3(-\mathbf{p},\mathbf{p}-\mathbf{k})}{\omega_2^2(k)}\langle\Psi|\rho_{\mathbf{q}}\rho_{\mathbf{k}-\mathbf{q}}\delta H^*\rho_{-\mathbf{p}}\rho_{\mathbf{p}-\mathbf{k}}|\Psi\rangle, \tag{4.1}$$

$$\frac{\delta F_t}{\delta\omega_3(\mathbf{q},\mathbf{k}-\mathbf{q})}\Big|_{g,u_3,\omega_2} = 0 = \langle\Psi|\rho_{\mathbf{q}}\rho_{\mathbf{k}-\mathbf{q}}\delta H^*\rho_{-\mathbf{k}}|\Psi\rangle + \frac{1}{N}\sum_{\mathbf{p}} \frac{\omega_3(-\mathbf{p},\mathbf{p}-\mathbf{k})}{\omega_2(k)}\langle\Psi|\rho_{\mathbf{q}}\rho_{\mathbf{k}-\mathbf{q}}\delta H^*\rho_{-\mathbf{p}}\rho_{\mathbf{p}-\mathbf{k}}|\Psi\rangle, \tag{4.2}$$

where $\epsilon^*(k) \equiv \epsilon(k)\tanh[\beta\epsilon(k)/2]$ and $\delta H^* \equiv H - E_0 - \epsilon^*(k)$. The $p = q$ term can be separated out of the summations in

Eqs. (4.1) and (4.2). The ratio of $\omega_3(\mathbf{p},\ \mathbf{k}-\mathbf{p})\ /\ \omega_2(k)$ can then be solved for by iterating Eq. (4.2). Substituting the resulting expression into Eq. (4.1) and keeping only the leading contribution yields a finite-temperature generalization of the energy expression obtained in Brillouin-Wigner perturbation theory:

$$\epsilon(k)=\frac{\epsilon_0(k)}{S(k)}\coth[\beta\epsilon(k)/2]+\frac{1}{Z_t^2N}\sum_{\mathbf{q}}\frac{|\langle\Psi|\rho_{\mathbf{q}}\rho_{\mathbf{k}-\mathbf{q}}\delta H\rho_{-\mathbf{k}}|\Psi\rangle|^2\coth[\beta\epsilon(k)/2]}{S(k)S(\mathbf{k}-\mathbf{q})S(q)[\epsilon^*(k)-\epsilon_{\mathrm{BF}}(q)-\epsilon_{\mathrm{BF}}(\mathbf{k}-\mathbf{q})]},\tag{4.3}$$

where $\delta H\equiv H-E_0-\epsilon_{\mathrm{BF}}(k)$ and $\epsilon_{\mathrm{BF}}(k)\equiv\epsilon_0(k)/S(k)$. In obtaining this result we used

$$\frac{1}{Z_t}\langle\Psi|\rho_{\mathbf{q}}\rho_{\mathbf{k}-\mathbf{q}}\delta H^*\rho_{-\mathbf{q}}\rho_{\mathbf{q}-\mathbf{k}}|\Psi\rangle\approx S(p)S(\mathbf{k}-\mathbf{q})[\epsilon_{\mathrm{BF}}(q)+\epsilon_{\mathrm{BF}}(\mathbf{k}-\mathbf{q})-\epsilon^*(k)].\tag{4.4}$$

The matrix element in the energy numerator can be written in the computationally convenient form

$$\frac{1}{Z_t}\langle\Psi|\rho_{\mathbf{q}}\rho_{\mathbf{k}-\mathbf{q}}\delta H\rho_{-\mathbf{k}}|\Psi\rangle=\frac{\hbar^2N}{2m}\{k^2+\mathbf{k}\cdot(\mathbf{k}-\mathbf{q})[S(q)-1]+\mathbf{k}\cdot\mathbf{q}[S(\mathbf{k}-\mathbf{q})-1]\}-\epsilon_{\mathrm{BF}}(k)S_3(\mathbf{q},\mathbf{k}-\mathbf{q},-\mathbf{k}),\tag{4.5}$$

where

$$S_3(\mathbf{q},\mathbf{k}-\mathbf{q},-\mathbf{k})\equiv\frac{1}{Z_t}\langle\Psi|\rho_{\mathbf{q}}\rho_{\mathbf{k}-\mathbf{q}}\rho_{-\mathbf{k}}|\Psi\rangle.\tag{4.6}$$

Similarly, variation with respect to $g(r)$ and u_3 produces two EL equations that are coupled nontrivially by the ω and u_3. As a first approximation we break the coupling by assuming that terms in the free energy that contain ω_3 can be neglected. For that case, evaluation of the EL equation for u_3, i.e.,

$$\left.\frac{\delta F_t}{\delta\tilde{u}_3(\mathbf{k}_1,\mathbf{k}_2,\mathbf{k}_3)}\right|_{g,\omega_2,\omega_3}=0,\tag{4.7}$$

is completely equivalent to the zero-temperature calculation.[22] We simply state the result

$$\tilde{u}_3(\mathbf{k}_1,\mathbf{k}_2,\mathbf{k}_3)\approx-\delta_{\mathbf{k}_1+\mathbf{k}_2+\mathbf{k}_3,\mathbf{0}}\times\frac{\mathbf{k}_1\cdot\mathbf{k}_2\tilde{X}(k_1)\tilde{X}(k_2)+\text{cyc. perm.}}{k_1^2/S(k_1)+k_2^2/S(k_2)+k_3^2/S(k_3)},\tag{4.8}$$

where $\tilde{X}(k)=1-1/S(k)$. In this form the temperature dependence of u_3 comes entirely through the $S(k)$. This expression for u_3 was shown by Chang and Campbell[8] to yield the correct density dependence for $\epsilon(k)$ in their zero temperature BW perturbation calculation of the spectrum. The connection to the energy numerator [Eq. (4.5)] is given by the approximation

$$S_3(\mathbf{k}_1,\mathbf{k}_2,\mathbf{k}_3)\approx\delta_{\mathbf{k}_1+\mathbf{k}_2+\mathbf{k}_3,\mathbf{0}}\times S(k_1)S(k_2)S(k_3)[1+\tilde{u}_3(\mathbf{k}_1,\mathbf{k}_2,\mathbf{k}_3)].\tag{4.9}$$

Omitting ω_3 in Eq. (3.18) reduces ω_2 back to the form used by Campbell *et al.*,[13]

$$n(k)[n(k)+1]=\omega_2(k)S(k).\tag{4.10}$$

We now evaluate the variation of the free energy with respect to $g(r)$. The result can be expressed conveniently in terms of a finite-temperature particle-hole interaction:

$$S(k)=\sqrt{\frac{\epsilon_0(k)+4\epsilon^*(k)S(k)n(k)[n(k)+1]}{\epsilon_0(k)+2\tilde{v}_{p-h}(k)}},\tag{4.11}$$

where $\tilde{v}_{\text{p-h}}(k)$ is the Fourier transform of

$$v_{\text{p-h}}(r)=g(r)[v(r)+\Delta v(r)]+\frac{\hbar^2}{m}[\nabla\sqrt{g(r)}]^2+[g(r)-1][w(r)+v^*(r)],\tag{4.12}$$

and

$$\Delta v(r)=\frac{2}{\rho}\left.\frac{\delta U_{\Delta u}}{\delta g(r)}\right|_{u_3,\omega_2,\omega_3}\tag{4.13}$$

is the correction term due to three-body and elementary diagrams. $w(r)$ is the induced interaction

$$\tilde{w}(k)=-\tfrac{1}{2}\epsilon_0(k)[2S(k)+1][S(k)-1]^2S^{-2}(k),\tag{4.14}$$

and $v^*(r)$ is a contribution from the entropy

$$-T\left.\frac{\delta\mathcal{S}_t}{\delta g(r)}\right|_{u_3,\omega_2,\omega_3}\equiv v^*(r)=\frac{1}{(2\pi)^3\rho}\int d\mathbf{k}\,e^{i\mathbf{k}\cdot\mathbf{r}}\epsilon^*(k)\frac{n(k)[n(k)+1]}{S(k)}.\tag{4.15}$$

Equations (4.3), (4.11), and (4.12), along with the HNC equations [Eqs. (3.9) and (3.10)], provide a closed set of equations that can be evaluated numerically. The solutions are discussed in Sec. VI. First we comment on the thermodynamic functions, which we calculate.

V. OPTIMAL THERMODYNAMIC FUNCTIONS

Perhaps the greatest importance of the present approach is that it allows thermodynamic functions to be calculated from a purely microscopic basis. This presents us with a unique opportunity to study the microscopic mechanisms, which are responsible for the thermodynamic behavior of the system.

Using the decomposition for the optimal internal energy in Eq. (3.3), it is apparent that, with Eqs. (3.4),

(3.5), and (4.8), $U_2 + U_{\Delta u}$ is completely specified. Furthermore, using the same approximations that lead to Eq. (4.11), one finds easily that the U_ω contribution to the internal energy [Eq. (3.12)] reduces to

$$U_\omega = \frac{1}{N}\sum_{\mathbf{k}} \epsilon^*(k) n(k)[n(k)+1], \tag{5.1}$$

Eq. (5.1) and the optimal entropy [Eq. (3.19)], completely determine the optimal Helmholtz free energy [Eq. (1.1)].

Another quantity of interest is the isothermal sound velocity c. In the present formalism, c is most easily obtained from the long-wavelength limit of the particle-hole interaction:

$$\tilde{v}_{\text{p-h}}(0) = mc^2. \tag{5.2}$$

The vanishing of c signals that the system has become mechanically unstable against long-wavelength fluctuations; the system can no longer support phonons. This instability corresponds to a divergence of the isothermal compressibility κ_T:

$$\frac{1}{\rho\kappa_T} \equiv \left.\frac{\partial p}{\partial \rho}\right|_T = mc^2, \tag{5.3}$$

where p is the pressure. Similar to the calculation of Campbell *et al.*,[13] at finite temperature, the long-wavelength limit of $S(k)$ [Eq. (4.11)] is related to c by

$$S(0) = \frac{1}{\beta mc^2}. \tag{5.4}$$

The locus of points in the temperature-density plane defined by the diverging compressibility is the thermodynamic spinodal curve. In the following section we discuss the effects that the spectrum and distribution functions have on the spinodal curve.

VI. RESULTS AND DISCUSSION

Before presenting our results we establish a nomenclature corresponding to the various approximations that can be invoked for solving the full Euler-Lagrange equations. The radial distribution function $g(r)$ and static structure function $S(k)$ can be generated by various approximate solutions of the HNC equations [Eqs. (3.9) and (3.10)]. We let HNC-0 denote the approximation that neglects elementary diagrams [$E(r) = 0$] in the HNC equations. This approximation is improved by keeping a portion of the fourth- and fifth-order elementary diagrams; the HNC-5 approximation. Including u_3 in the distribution functions is denoted by U_3. To distinguish the various approximations for the spectra we adopt the following nomenclature.

Feynman HNC-5-U_3 level. We will refer to the first term of Eq. (4.3) as the (finite-temperature) Feynman spectrum:

$$\epsilon(k) = \frac{\epsilon_0(k)}{S(k)} \coth[\beta\epsilon(k)/2]. \tag{6.1}$$

In this limit Eq. (4.11) reduces to

$$S(k) = \frac{\coth[\beta\epsilon(k)/2]}{\sqrt{1 + 2\tilde{v}_{\text{p-h}}(k)/\epsilon_0(k)}}. \tag{6.2}$$

These equations are consistent with setting ω_3 equal to zero in the trial density matrix. The radial distribution and static structure functions are generated in the HNC-5-U_3 approximation. Throughout this work, when the distribution functions are calculated at the HNC-5-U_3 level, the same is true for $v_{\text{p-h}}(r)$. For example, in the HNC-5 approximation $\Delta v(r)$ is calculated by taking functional derivatives of the appropriate fourth- and fifth-order elementary diagrams. A detailed discussion is given in Ref. 22.

The *Feynman HNC-5*, *Feynman HNC-0-U_3*, and *Feynman HNC-0 levels.* These are similar to the Feynman-HNC-5-U_3 level but with u_3, elementary diagrams, or both set equal to zero, respectively. The Feynman-HNC-0 level was previously investigated by Campbell *et al.*[13]

CBF-HNC-5-U_3 level. At this level all distribution functions are calculated in the HNC-5-U_3 approximation. The spectrum is obtained by the full self-consistent solution of Eq. (4.3). The S_3 dependence in the energy numerator [Eq. (4.5)] follows from Eqs. (4.8) and (4.9).

Having specified our nomenclature, we now proceed to present and discuss our results. We begin with the microscopic functions; the distribution functions, excitation energies, and the particle-hole interaction.

A. Radial distribution and static structure functions

The effects of including elementary diagrams and three-body correlations in the static distribution functions is well understood at zero temperature.[22,23] Compared to a $g(r)$ calculated from an HNC-0 approximation, a $g(r)$ determined at the HNC-5-U_3 level has an enhanced first-neighbor peak followed by a slightly deepened first trough. At finite temperatures, one can again examine these effects. The radial distribution functions for two temperatures at SVP are shown in Fig. 1. They are calculated at the CBF-HNC-5-U_3 level. Also shown in the same figure are the experimental points of Svensson *et al.*[25] The good agreement with experiment is readily apparent. Although not shown in the figure, the $g(r)$ generated at the Feynman-HNC-0 level, at $T = 1.0$ K, shares the same behavior as the zero-temperature functions: The Feynman-HNC-0 level $g(r)$ has first-peak and trough values of 1.34 and 0.91 contrasted to values of 1.41 and 0.87 at the CBF-HNC-5-U_3 level. This shift in magnitude is essentially the same as that observed at zero temperature. Consequently, finite-temperature effects are nearly the same for the two different levels of approximation used to calculate $g(r)$.

The temperature and density dependence of the static structure function $S(k)$ are shown in Figs. 2 and 3. $S(k)$ in both figures are calculated at the CBF-HNC-5-U_3 level. Only quantitative differences exist between these $S(k)$ and those determined at the Feynman-HNC-0 level. We refer the reader to Ref. 13 for a detailed discussion on the temperature and density dependence of $S(k)$.

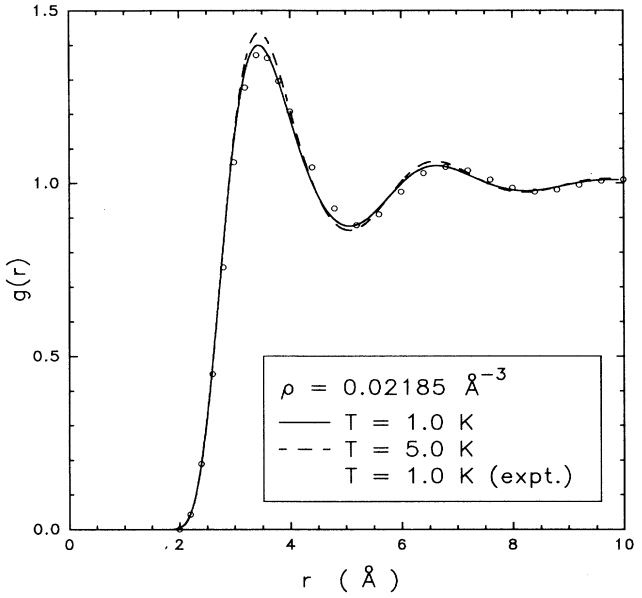

FIG. 1. The experimental and theoretical radial distribution function. The experimental points are taken from Ref. 25, and the theoretical curves are calculated at the CBF-HNC-5-U_3 level.

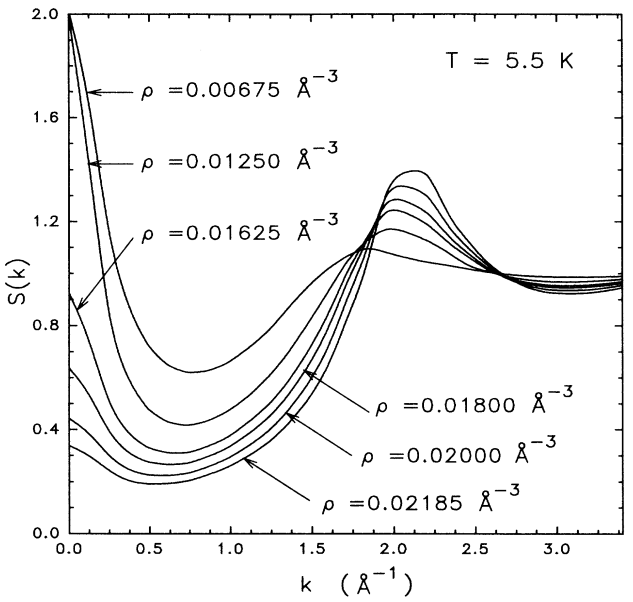

FIG. 3. The density dependence of the static structure function. The curves are calculated at the CBF-HNC-5-U_3 level.

B. Elementary-excitation energies

At zero temperature Krotscheck[11] used linear response theory and variational theory to provide a rigorous means for determining the low-lying excitations. The excitations arise from subjecting the ground state of the helium liquid to a time-dependent perturbing field. At finite temperature, a properly constructed density matrix already incorporates the physics of the low-lying excited states. In that case, thermal fluctuations replace the role of the time-dependent perturbing field of the zero-temperature calculation. As the temperature is reduced, Eq. (4.3) evolves to the zero-temperature spectrum of Chang and Campbell.[8] This shows that one may excite the same quasiparticle excitations by either thermally *flashing* and *quenching* the system or, at zero temperature, by perturbing the system as in a neutron-scattering experiment. We believe that a major accomplishment of the present work is the derivation of Eq. (4.3). The fact that the next-higher-order term, after the Feynman spectrum [Eq. (4.3)], is the CBF three-phonon vertex correction, provides a convincing statement about the validity of relating the spectrum via the quasiparticle momentum distribution, to the trial entropy.

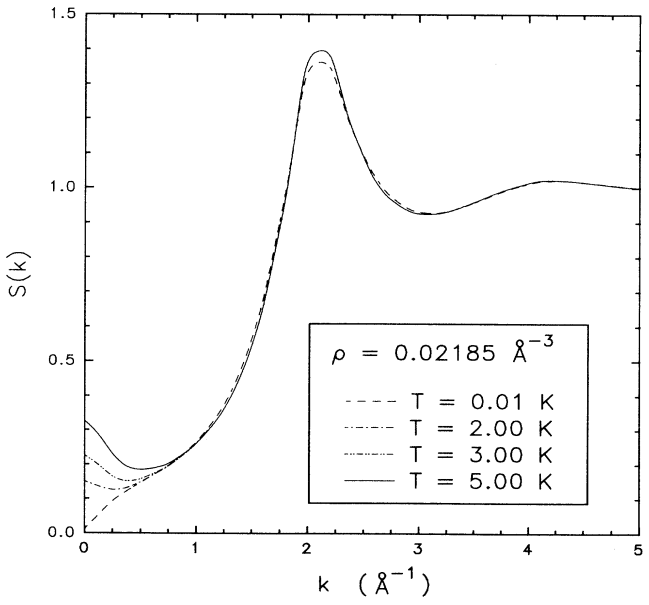

FIG. 2. The temperature dependence of the static structure function. The curves are calculated at the CBF-HNC-5-U_3 level.

Three-phonon scattering processes have several important and well-studied effects on the zero-temperature spectrum. As is apparent from the transition-matrix element,

$$\langle \Psi | \rho_{\mathbf{q}} \rho_{\mathbf{k}-\mathbf{q}} \delta H \rho_{-\mathbf{k}} | \Psi \rangle, \tag{6.3}$$

two types of processes are involved: the dissociation of an excitation into two excitations and the time-reversed process of two excitations coalescing into a single excitation. For a given energy ω and momentum transfer $\mathbf{k}$, conservation of energy and momentum determine the allowed two-particle density of states for these three phonon scattering events.[26] The self-consistency imposed on ω by Eq. (4.3), i.e.,

$$\epsilon^*(k) = \epsilon_{\mathrm{BF}}(k) + \Sigma^*(k, \omega = \epsilon^*(k)), \tag{6.4}$$

restricts greatly the allowed scattering events. The CBF

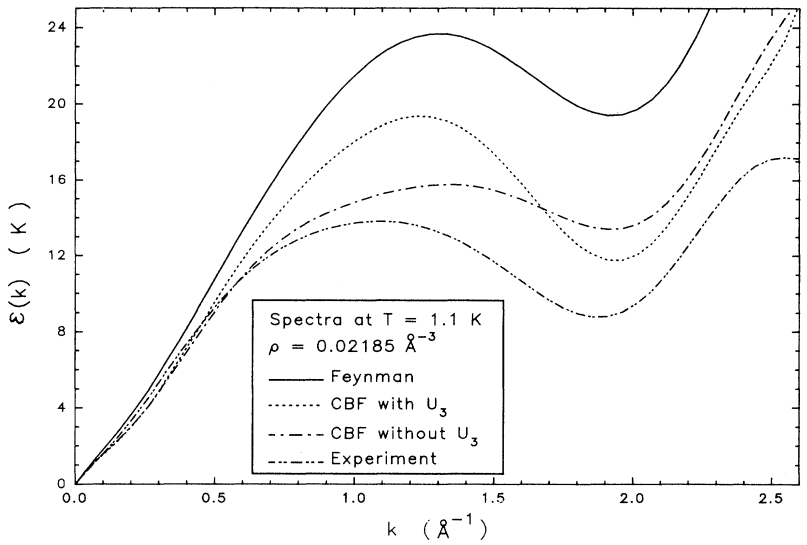

FIG. 4. Theoretical and experimental elementary-excitation energies. The experimental data is taken from Ref. 27. The Feynman curve is calculated at the Feynman-HNC-0 level. The two CBF curves are calculated at the CBF-HNC-5-U_3 level; however, in one case the u_3 dependence in the energy numerator of Eq. (4.5) is dropped.

correction term does have an appreciable effect on the spectrum for most momenta, however. Figure 4 shows a comparison of spectra at $T = 1.1$ K and SVP. The experimental spectrum is that of Cowley and Woods,[27] and the Feynman and CBF spectra are calculated from Eq. (6.1) and Eq. (4.3), respectively. We also show the CBF spectrum, but calculated with u_3 set equal to zero in the energy numerator [Eq. (4.9)]. Excluding u_3 in the energy numerator actually produces better agreement with experiment near the maxon, but including u_3 improves the agreement near the roton and should produce a better density dependence. We remind the reader that our u_3 dependence has been greatly simplified by our decoupling approximation that lead to Eq. (4.8). This fact may produce an inconsistency in our approximations. In fact, these results are somewhat similar to the findings of Manousakis and Pandharipande.[6] In a zero-temperature BW-type calculation, those authors found that using a Green's-function-Monte Carlo (GFMC) generated $g(r)$ as input gave considerably poorer agreement with experiment, near the maxon, than a $g(r)$ generated by a variational calculation. Consequently, using our $g(r)$ determined at the HNC-5-U_3 level may, in fact, require more precise approximations, than the corresponding HNC-0 level $g(r)$.

The three-phonon processes are clearly most important for momenta exceeding that of the maxon. The temperature and density dependence of the spectrum are shown in Figs. 5–7 . For clarity the density dependence of the spectrum has been divided into plots for the high- and low-density portions of the phase diagram. Below 2 K the spectrum is very nearly temperature independent. As in the Feynman-HNC-0 level calculation,[13] the temperature dependence of the roton gap energy is qualitatively incorrect; it increases with increasing temperature.

Another aspect of the multiphonon contribution, which will be considered more fully in our discussion of the entropy, is the rapid *jump* and then leveling off of $\epsilon(k)$ for

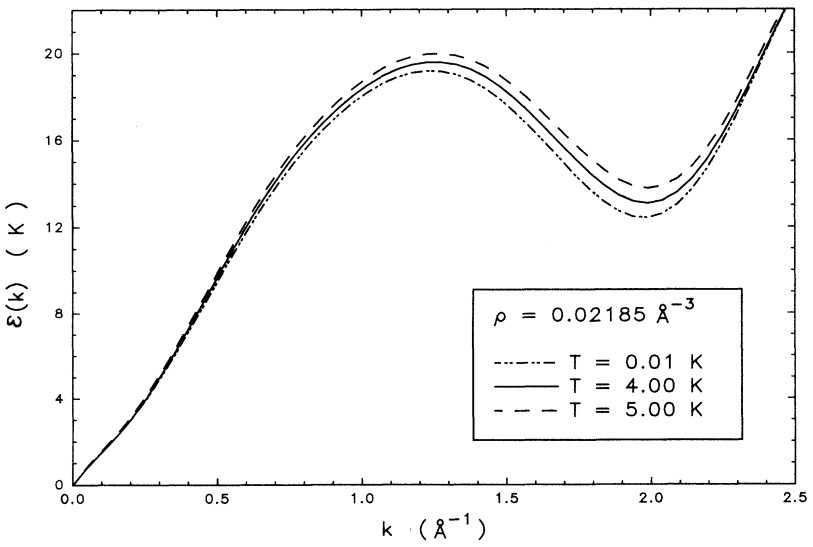

FIG. 5. The temperature dependence of the elementary-excitation energies. The curves are calculated at the CBF-HNC-5-U_3 level.

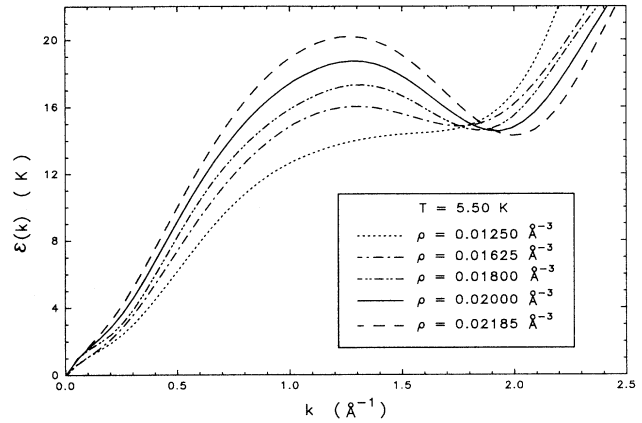

FIG. 6. The density dependence of the elementary-excitation energies in the high-density regime. The curves are calculated at the CBF-HNC-5-U_3 level.

momentum above the roton minimum. This behavior is best displayed in Fig. 7. The jump in the spectrum can be traced to an abrupt change in the CBF correction term associated with a predominance of intermediate scattering states yielding a sign change in the energy denominator [Eq. (4.3)] when going from low to high momentum $\mathbf{k}$. The spectrum leveling can be attributed to the dissociation processes mentioned above. Intermediate states with a large single-particle density of states (the maxon and roton) will be most influential. For example, near SVP, leveling occurs at energies approximately twice the roton gap energy.

One final point needs to be made concerning the multiphonon corrections. If one associates the CBF correction term with a single-particle self-energy as in Eq. (3.21) or (6.4), then formally, the vanishing of the energy denominator is accompanied by the emergence of a complex self-energy, $\mathrm{Im}\Sigma$. Iterating the full (complex) spectrum will shift the energy pole off the real-energy axis by an amount proportional to $\mathrm{Im}\Sigma$. The lifetime of the excitation is inversely proportional to $\mathrm{Im}\Sigma$. This of course is simply the statement that the multiphonon excitations provide a decay mechanism for the quasiparticle states. In the present work we have not calculated $\mathrm{Im}\Sigma$. Consequently, this portion of the spectrum is only qualitatively correct.

C. Particle-hole interaction

As seen in the present formalism, the particle-hole interaction plays a fundamental role in determining the static properties of the system. It is also the primary driving interaction in the calculation of the dynamic response function, $\chi(k,\omega)$. In Fig. 8, $\tilde{v}_{\mathrm{p\text{-}h}}(k)$ is displayed over a broad range of densities for $T = 5.5$ K. The mechanical stability of the system decreases as the isotherm is traversed from high densities to densities near the spinodal. Moving away from the spinodal, on the low-density side, increases the mechanical stability again. This is the cause of the crossing at zero wave vector observed at the lowest two densities shown in Fig. 8.

The microscopic quantities previously discussed provide the input for calculations of the thermodynamic functions. We now discuss the entropy, Helmholtz free energy, and isothermal sound velocity. These functions are all determined at the CBF-HNC-5-U_3 level. We close this section with a discussion of the thermodynamic spinodal curve.

D. Trial entropy

An obvious benefit from having a simple ansatz for the trial entropy [Eq. (3.19)] is that the microscopic mechanisms, which govern the entropic behavior of the fluid, are quite transparent. The link, of course, is provided by the elementary-excitation energies $\epsilon(k)$. Figure 9 is a plot of entropy density isotherms for densities up to 0.021 85 Å^{-3}. The thermodynamic spinodal curve is also shown. The view taken in the present work is that Eq. (3.19), which is exact in the limit of noninteract-

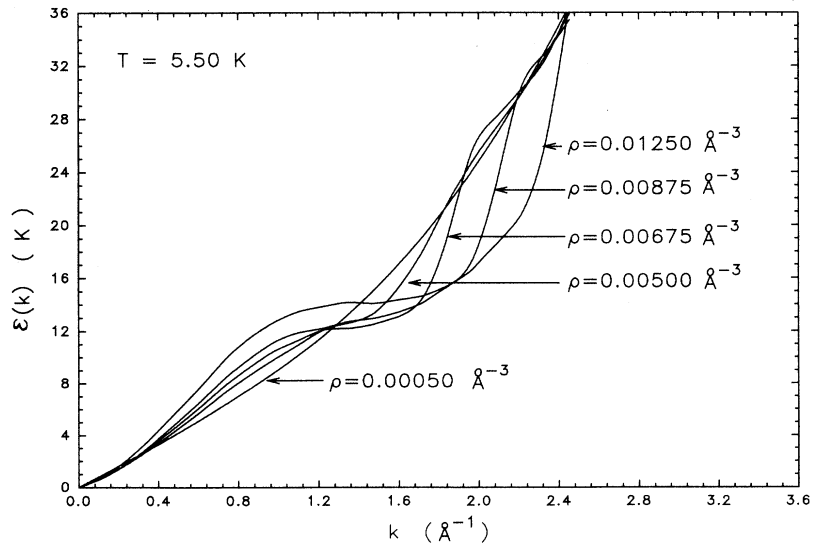

FIG. 7. The density dependence of the elementary-excitation energies in the low-density regime. The curves are calculated at the CBF-HNC-5-U_3 level.

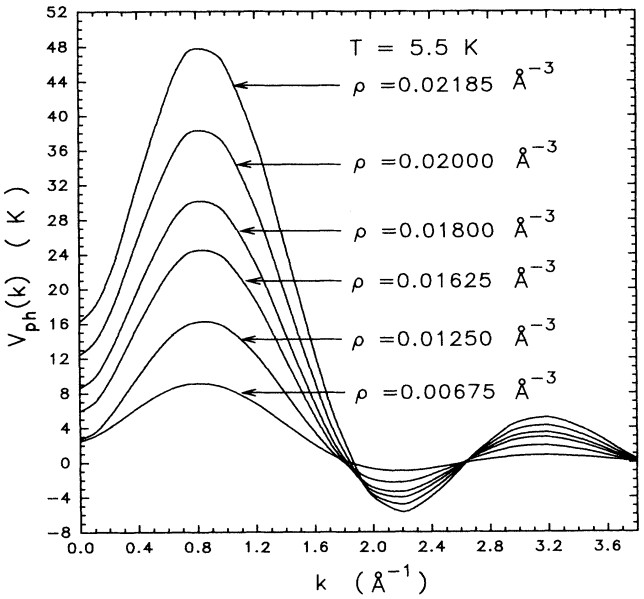

FIG. 8. The density dependence of the particle-hole interaction. The curves are calculated at the CBF-HNC-5-U_3 level.

ing Bose quasiparticles, is adequate when the number of excitations per unit volume are small. For the liquid phase (the high-density side of the thermodynamic spinodal curve) this condition places an upper limit on the temperature for which Eq. (3.19) is reliable. Partial support of this view can be found in the comprehensive tables of Brooks and Donnelly,[28] where the entropy for temperatures up to 2.2 K and positive pressures up to 25 atm is calculated from Eq. (3.19) when experimental data was not available. At still higher temperatures, one must expect quasiparticle interactions to be increasingly

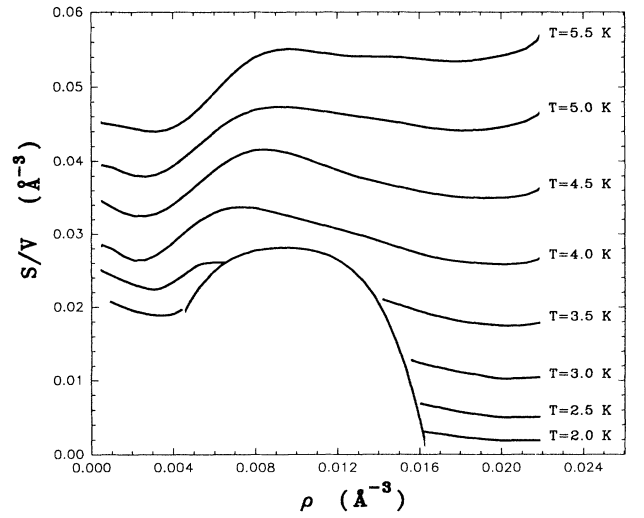

FIG. 9. Entropy density isotherms calculated at the CBF-HNC-5-U_3 level. The theoretically determined spinodal curve is also shown.

prevalent. For this case, one cause for our results to deviate from the experimental entropy can be attributed to the breakdown of Eq. (3.19). Parenthetically, it is for this reason that Clements and Campbell[21] were lead to a reformulation of the variational problem that precluded the need for introducing an explicit ansatz for the entropy.

Even within the domain of validity of Eq. (3.19), discrepancies between our entropy and the experimental value arise because of spectra differences. For example, the experimentally determined $\epsilon(k)$ at 1.1 K and SVP of Cowley and Woods has a roton energy gap of $\Delta = 8.68$ K. This is to be contrasted with $\Delta = 20.0$ K for the Feynman spectrum and $\Delta = 12.18$ K for the CBF spectrum. These spectra lead to entropies of 0.029 J g^{-1} K^{-1}, 0.008 J g^{-1} K^{-1}, and 0.014 J g^{-1} K^{-1} for the experimental,[28] Feynman, and CBF spectra, respectively.

The multiphonon contributions introduce new physics into the entropy that is not present at the *Feynman level.* Most noticeable is the substantial shift in the entropy density on the low-density side of the spinodal curve. For example, for the $T = 5.5$ K isotherm, the shift occurs approximately between low and high densities of $\rho_L = 0.005$ Å^{-3} and $\rho_H = 0.00875$ Å^{-3}, respectively. The origin of the entropy shift is the changing nature of the spectrum (Fig. 7) that occurs as the density changes from ρ_L to ρ_H. Above ρ_H the spectra are largely influenced by multiphonon processes in the CBF correction to $\epsilon(k)$. Below ρ_L multiphonon processes are insignificant. In fact, for the densities less than ρ_L the entropy density in Fig. 9, matches the *Feynman level* values. Above ρ_H the nature of the entropy isotherms differ considerably for the two different levels of calculation; the rather flat entropy density isotherms in Fig. 9 should be contrasted with the Feynman isotherms, which are always monotonically decreasing functions of increasing density. Experimentally, the $T = 5.5$ K entropy density isotherm vanishes for low density and increases with increasing density.

The values of the entropy in the vicinity of the entropy density shift are likely to be quite susceptible to error because of the neglect of the imaginary part of the self-energy, as was discussed in Sec. VI B. In that density regime it is apparent from Fig. 7 that multiphonon-dissociation processes (the flattening of the spectrum for momenta above the jump) shift toward momenta that are highly relevant in determining the behavior of the the momentum distribution, $n(k)$, and ultimately the entropy. Finally we mention that in our numerical investigations of this region we also observed that it was possible to iterate along "metastable-like" solutions, and care had to be taken to choose the true isotherm that minimized the free energy. Once again, further investigation of this effect is not warranted at the present because incorporating the complex self-energy is expected to have a significant impact in this region.

E. Helmholtz free energy

The Helmholtz free-energy-density isotherms are shown in Fig. 10. At the lowest densities, the free-energy

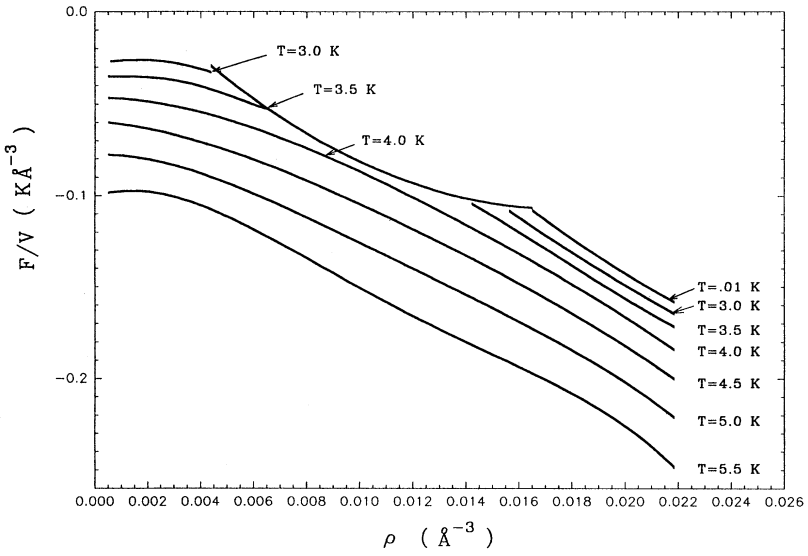

FIG. 10. Helmholtz free-energy density isotherms calculated at the CBF-HNC-5-U_3 level. The theoretically determined spinodal curve is also shown.

density reduces to the Feynman-HNC-0 level values. This is a consequence of the results of Sec. VI D and the fact that the internal energy reduces to the Jastrow-HNC-0 value at very low densities. Near SVP, the free-energy density is appreciably more negative than the Feynman-HNC-0 values. The addition of the CBF correction, elementary diagrams, and three-body correlations, all contribute to the lowering of the free energy near SVP. The zero-temperature free-energy isotherm has a minimum at $\rho \approx 0.021\,85$ Å^{-3} and a value of -7.2 K.

F. Isothermal sound velocity

The isothermal sound velocity, c is calculated directly from the long-wavelength limit of the particle-hole interaction [Eq. (5.2)]. Figure 11 reveals that c is qualitatively similar to the sound velocities calculated by Senger *et al.*[17] Rather than repeating the discussion found in Ref. 17, we mention only those facts that differ from their calculation.

At the CBF-HNC-5-U_3 level there exists a rather substantial uncertainty in the values of c for $\hbar c \lesssim 1.0$ Å K. For the most part, $\hbar c$ shown in Fig. 11 that are less than 1.0 Å K are obtained by extrapolating from values neighboring $\hbar c = 1.0$ Å K. The reason for the difficulty is entirely technical and can be attributed primarily to complications arising in the elementary diagram calculation. In principle, this problem can be reduced by using a much larger real-space box size. In this work, our objective was to study a large amount of phase space rather than to strive for a precise mapping of the spinodal curve, which is defined by the locus of points where c vanishes. At the CBF-HNC-5-U_3 level, we estimate the uncertainties in the densities of the location of the spinodal curve

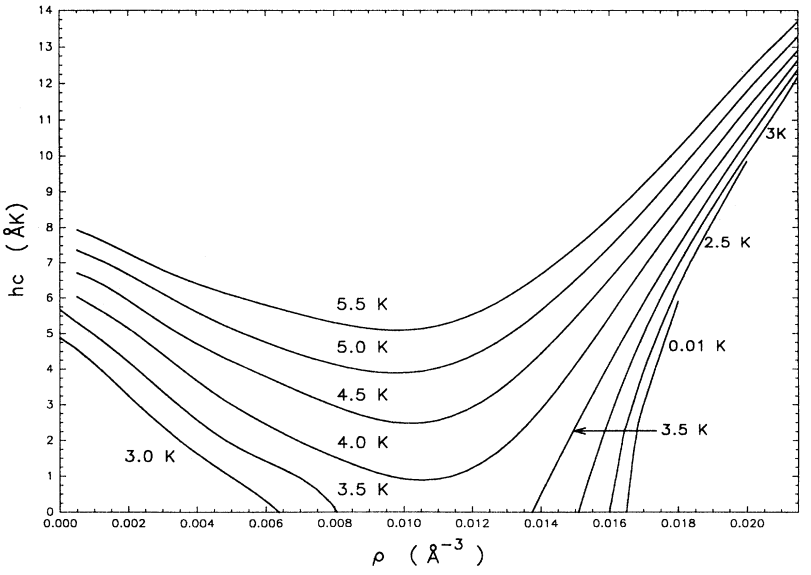

FIG. 11. Isothermal sound velocity isotherms calculated at the CBF-HNC-5-U_3 level.

to be ± 0.0005 Å^{-3} for the gas side and ± 0.0002 Å^{-3} on the liquid side. The uncertainty in the temperature is estimated at ± 0.2 K. At the *Feynman level*, the uncertainties are considerably smaller. The uncertainty associated with locating the spinodal curve is considerably less for the other approximations.

G. Spinodal curve

Finally, the role of the spectrum and the distribution functions on determining the location of the spinodal curve is investigated. The results are shown in Fig. 12. Each curve represents a different approximation to the spinodal curve. The density and temperature corresponding to the peak values are the critical point values (T_c, ρ_c). The experimental values for ^{4}He are at $T_c \approx 5.3$ K and $\rho_c \approx 0.010$ Å^{-3}. The best agreement with the experimental critical values is obtained at the Feynman-HNC-0-U_3 level. This result was anticipated from the earlier work in Ref. 17, since an increase in T_c indicates a more strongly bound system, and adding three-body correlations increases the binding energy of the system by a substantial amount. What is less obvious is the effect of adding elementary diagrams into the calculation. The elementary-diagram contribution reduces T_c, independent of the choice of the spectrum. In the case of the Feynman spectrum, there is a net increase in the values of (T_c, ρ_c) when both elementary-diagram and three-body correlations are taken into account. In principle, our best calculation of the spinodal curve, the CBF-HNC-5-U_3 level, differs the most from the experimental T_c, while ρ_c is improved. There seems to be a fortuitous agreement with the experimental data at the *Feynman level*. In the next section we will point out, that view may be incorrect.

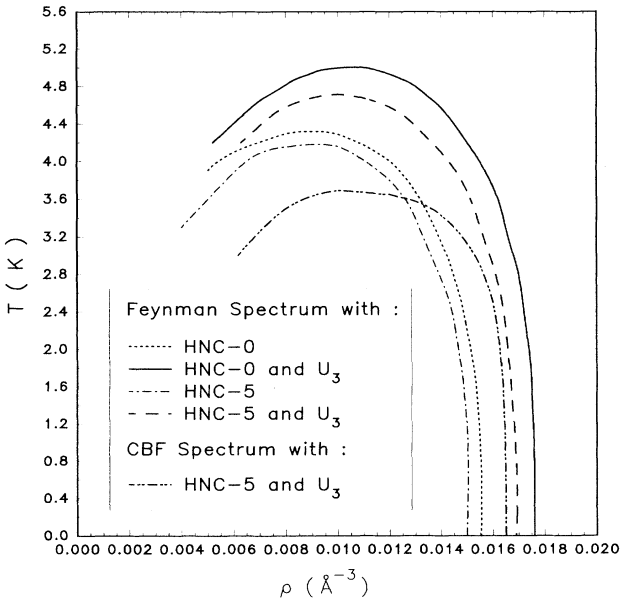

FIG. 12. Different theoretical approximations to the thermodynamic spinodal curve.

VII. CONCLUDING REMARKS

Clearly, including three-body correlations, u_3 and ω_3 in the PRCJ density matrix have important consequences on the microscopic and thermodynamic functions of a strongly correlated Bose liquid. For liquid densities, and temperatures less than 2.0 K, the microscopic and thermodynamic functions are most certainly in better agreement with the experimental results. In that regime, the CBF corrections to the spectrum make a substantial difference, but still leave room for further improvement. While higher-order CBF terms can be systematically calculated, it would be a formidable task to do so.

Above 2.0 K, the extended PRCJ density matrix is qualitatively incorrect because single-particle (SP) states are not properly accounted for. Altering the PRCJ density matrix to include the normal phase of the Bose liquid has been pursued.[15,17,20] Unfortunately, those results are inconclusive in regard to the quantitative aspects of the SP states. A simpler but illuminating calculation, which should be qualitatively correct for $T \approx T_\lambda$, has recently been reported by Blendowske and Fliessbach.[29] Their results indicate that the anomalous increase in the first peak of the static structure function for $T < T_\lambda$, and then its reversal for higher temperatures, is caused by the temperature dependence of the SP states. We would modify their conclusions somewhat, in that we find collective excitations probably dominate the anomalous temperature dependence of $S(k)$ for $T < T_\lambda$, while above T_λ, the SP states and the attractive nature of roton-roton interactions are responsible for the reversal of the behavior. This actually does not disagree with the findings of Blendowske and Fliessbach, since their SP behavior below T_λ produces a temperature anomaly for $S(k)$ that is substantially less than the experimentally observed anomaly.

The role of the SP states is expected to be of increasing importance with decreasing density. The fact that our free energy and entropy densities do not vanish at zero density, can of course, be attributed to our neglect of the relevant SP physics. From this work it seems reasonable that the thermodynamic phase diagram for the correlated Bose fluid (at temperatures in the neighborhood of those studied here) can be thought of as consisting of essentially four regions. Each region is mediated by somewhat different physics. At very low densities (to the far left of the spinodal curve in Fig. 12) SP states dominate the physics. At higher densities and above several degrees Kelvin, SP states remain important, but collective effects become increasingly prevalent. A superficial glance of the CBF-HNC-5-U_3 level spinodal curve in Fig. 12 may lead one to believe that collective modes miss much of the relevant physics in that regime. That interpretation may be wrong. If multiphonon contributions had fully diminished slightly to the right of the transition temperature rather than to the left (Fig. 9) and the elementary diagram had shown a similar increase in falloff then the location of the spinodal curve would correspond to the Feynman-HNC/0-U_3 level curve. This change in the density dependence of the multiphonon and elementary diagram contributions is clearly within

the range that could be achieved by a more precise calculation. Consequently, we propose that the second region extends between the approximate densities of 0.001 Å^{-3} and 0.015 Å^{-3} and is mediated by SP states and Feynman single-phonon excitations. The third region encompasses still higher densities, and temperatures above the λ transition temperature. Multiphonon and SP excitations are both relevant. Below this temperature, in the fourth region, the SP states begin to lose their significance.

ACKNOWLEDGMENTS

The authors would like to thank T. Ainsworth for discussions on this work. The work was supported, in part, by the National Science Foundation under Contract Nos. PHY88-06265 and PHY91-08066, and the Texas Advanced Research Program under Grant No. 010366-012. Support from the Minnesota Supercomputing Insitute is gratefully acknowledged.

[1]W. G. Stirling and H. R. Glyde, Phys. Rev. B **41**, 4224 (1990).
[2]E. F. Talbot, H. R. Glyde, W. G. Stirling, and E. C. Svensson, Phys. Rev. B **38**, 11 229 (1988).
[3]A. D. B. Woods and E. C. Svensson, Phys. Rev. Lett. **41**, 974 (1978).
[4]H. R. Glyde and A. Griffin, Phys. Rev. Lett. **65**, 1454 (1990).
[5]S. T. Beliaev, Zh. Eksp. Teor. Fiz. **34**, 417 (1958) [Sov. Phys. JEPT **7**, 289 (1958)]; N. Hugenholtz and D. Pines, Phys. Rev. **116**, 489 (1959); J. Gavoret and P. Nozières, Ann. Phys. (N.Y.) **34**, 291 (1965); A. Griffen and T. H. Cheung, Phys. Rev. A **7**, 2086 (1973); P. Szépfalusy and I. Kondor, Ann. Phys. (N.Y.) **82**, 1 (1974).
[6]E. Manousakis and V. R. Pandharipande, Phys. Rev. B **30**, 5062 (1984).
[7]M. Saarela and J. Suominen, *Condensed Matter Theories*, edited by J. S. Arponen, R. F. Bishop, and M. Manninen (Plenum, New York, 1988), Vol. 3, p. 157; (private communication).
[8]C. C. Chang and C. E. Campbell, Phys. Rev. B **13**, 3779 (1976).
[9]D. K. Lee, Phys. Rev. **162**, 134 (1967).
[10]H. W. Jackson and E. Feenberg, Rev. Mod. Phys. **34**, 686 (1962).
[11]E. Krotscheck, Phys. Rev. B **31**, 4258 (1985).
[12]B. E. Clements, J. L. Epstein, E. Krotscheck, M. Saarela, and C. J. Tymczak, J. Low Temp. Phys. **89**, 585 (1992).
[13]C. E. Campbell, K. E. Kürten, M. L. Ristig, and G. Senger, Phys. Rev. B **30**, 3728 (1984); *Condensed Matter Theories*, edited by F. B. Malik (Plenum, New York, 1986), Vol. 1, p. 153.
[14]R. A. Aziz, V. P. S. Nain, J. C. Carley, W. L. Taylor, and G. T. McConville, J. Chem. Phys. **70**, 4330 (1979).
[15]C. E. Campbell and B. E. Clements, in *Elementary Excitations in Quantum Fluids*, Solid-State Sciences, Vol. 79, edited by K. Ohbayashi and M. Watabe (Springer-Verlag, New York, 1989); B. E. Clements, doctoral dissertation, University of Minnesota, 1988 (unpublished).
[16]C. E. Campbell and E. Feenberg, Phys. Rev. **188**, 396 (1969); J. W. Clark, in *Progress in Nuclear and Particle Physics*, edited by D. H. Wilkinson (Pergamon, Oxford, 1979), Vol. 2; C. E. Campbell, in *Progress in Liquid Physics*, edited by C. A. Croxton (Wiley, New York, 1978).
[17]G. Senger, M. L. Ristig, K. E. Kürten, and C. E. Campbell, Phys. Rev. B **33**, 762 (1986); *Condensed Matter Theories* (Ref. 13), p. 158.
[18]K. E. Kürten and M. L. Ristig, Phys. Rev. B **37**, 3359 (1988).
[19]K. A. Gernoth and M. L. Ristig, Phys. Rev. B **45**, 2969 (1992); K. Gernoth, Diplomarbeit, Univerität zu Köln, 1987 (unpublished).
[20]G. Senger and M. L. Ristig, *Condensed Matter Theories*, edited by V. C. Aguilera-Navarro (Plenum, New York, 1990), Vol. 5, 133; G. Senger, M. L. Ristig, C. E. Campbell, and J. W. Clark, Ann. Phys. (N.Y.) (to be published).
[21]B. E. Clements and C. E. Campbell, Phys. Rev. B **46**, 10 957 (1992).
[22]E. Krotscheck, Phys. Rev. B **33**, 3158 (1986).
[23]C. C. Chang and C. E. Campbell, Phys. Rev. B **15**, 4238 (1977).
[24]S. Battaini and L. Reatto, Phys. Rev. B **28**, 1263 (1983).
[25]E. C. Svensson, V. F. Sears, A. D. B. Woods, and P. Martel, Phys. Rev. B **21**, 3638 (1980).
[26]H. W. Jackson, Phys. Rev. A **4**, 2386 (1971).
[27]R. A. Cowley and A. D. B. Woods, Can. J. Phys. **49**, 177 (1971).
[28]J. S. Brooks and R. J. Donnelly, J. Phys. Chem. Ref. Data **6**, (1) 51 (1977).
[29]R. Blendowske and T. Fliessbach, J. Phys. Condens. Matter **4**, 3361 (1992).